Engineering with Computers (2009) 25:49–59
DOI 10.1007/s00366-008-0104-3

ORIGINAL ARTICLE

Estimation of vascular open configuration using finite element inverse elastostatic method

Xianlian Zhou · Jia Lu

Received: 15 February 2007 / Accepted: 11 September 2007 / Published online: 29 August 2008
© Springer-Verlag London Limited 2008

Abstract This paper presents a new method for predicting the open configuration of vascular organs. The method utilizes finite element inverse elastostatic formulations. The equilibrium boundary value problem is formulated on the homeostatic configuration, and is solved inversely to find the open, stress-free configuration. The method is non-invasive, and enables us to estimate the open configuration based on information that is readily available form in vivo measurements. Examples involving both axisymmetric and asymmetric geometries are presented to demonstrate the utility of the method.

Keywords Residual stress · Opening angle · Inverse method · Inverse elastostatics

1 Introduction

Since the discovery of residual stress in arteries [1–4], there have been many studies on the presence of residual stresses in soft tissue organs and their influence on organs' mechanical response [5–10]. In arteries, the residual stress is believed to homogenize the circumferential stress when the artery is under physiological pressure [2]. It has even been speculated that, due to the presence of the residual stress, the circumferential stress under the homeostatic pressure is nearly uniform across the wall thickness [11, 12]. The most commonly used method for describing residual stress in artery wall was proposed by Chuong and Fung [1]. The method builds on the experimental observation that an artery ring opens up to a cylindrical sector, which is approximately stress free, after a radial cut is applied to the wall. If the open sector geometry and the constitutive equation for the material are known, the residual stress in the intact (i.e., closed and unloaded) configuration can be determined from the boundary value problem (BVP) that governs the closing motion. The normal arterial deformation can be modeled by a superposition of two motions, an imaginary motion that closes the sector followed by a radial expansion that brings the artery from the intact ring to a pressurized configuration. In this manner, the residual stress is properly taken into account in a mechanical analysis.

The cut experiment remains perhaps the most reliable method for studying residual stress. However, it is a destructive process and hence not suited to certain applications. Many researchers have submitted methods for predicting the open configuration without performing the cut experiment. If one assumes that both the intact configuration and the open sector are perfectly cylindrical, and that the closing motion involves pure bending, the residual stress in the intact state can be derived as a function of the open sector geometry (the opening angle and radii) and other model parameters. If certain features of the residual stress or the residual strain field are known, the open sector geometry can be estimated. Van Dyke and Hoger [13] proposed an energy method for estimating the open sector from knowledge of the residual stress distribution in the intact configuration. Taber and Eggers [14] suggested a formula for predicting the opening angle from the knowledge of the circumferential stretch values at several radial locations in the intact state. The limitation in these methods is the requirement of a priori knowledge of the residual stress or strain, which is difficult to obtain in practical

X. Zhou · J. Lu (✉)
Department of Mechanical and Industrial Engineering,
Center for Computer Aided Design, The University of Iowa,
Iowa City, IA 52242-1527, USA
e-mail: jia-lu@uiowa.edu

applications (in [14], the residual strain was predicted from growth). Stalhand et al. [15] proposed an optimization approach in which the open sector geometry is identified, together with the elasticity parameters, by fitting the model response to the experimental pressure-diameter data. They also considered residual strains that may not be released by a single cut [16]. This approach, however, is limited to axisymmetric problems in which the residual stress varies only radially, and the distribution can be described using a limited number of parameters.

In this paper, we propose a new approach for predicting the open configuration of vascular organs. We assume that the homeostatic configuration, the corresponding pressure, and the constitutive equation for the material are known. The open configuration, which is assumed to be stress-free, is predicted using finite element inverse elastostatic formulations. It is known that, the initial configuration of an *elastic* material body can be found if a deformed state and the applied load are given. Govindjee and Mihalic [17, 18] established a paradigm of finding the initial configuration using the standard equilibrium BVP. Unlike some other inverse problems, the inverse elastostatic problem is well-posed [17]. The present authors have extended the inverse formulation, and applied it to the stress analysis of aneurysms based on patient-specific diagnostic images [19, 20]. Here, we take the homeostatic configuration of a vascular organ as given, and determine the open configuration resulted from a hypothetic cut applied to the homeostatic configuration. A critical step in this approach is to compute the pre-cut wall stress along the (hypothetic) cut boundary, because this stress field provides the traction boundary condition for the inverse problem. Motivated by a common speculation [11, 12], we assume that in the homeostatic state, the wall stress is uniform across the wall-thickness. As will be demonstrated later, this assumption enables us to determine the homeostatic wall stress in both cylindrical and asymmetric geometries.

The proposed method has several noteworthy attributes. First, it enables us to estimate the opening configuration using information that is readily obtainable by today's diagnostic tools. In practice, the homeostatic geometry of a vascular organ can be approximated by the average geometry over a cardiac-cycle, which can be extracted from medical imaging data. Second, the method does not require a priori knowledge of the residual stress (or strain) in the intact state; instead, the residual stress can be predicted once the open configuration is found. Third, the procedure is applicable to a certain family of asymmetric organs, although in this case the assumption that the open configuration is stress-free needs to be carefully evaluated. Lastly, the method suggests a non-invasive approach for taking into account the residual stress in vascular mechanics. For example, if the systolic arterial wall stress of a patient is to be estimated, one can compute the open configuration using this inverse approach, and then determines the systolic stress by solving a forward problem.

We present two examples to illustrate the procedure and utility of the proposed method. The first example deals with a perfectly cylindrical artery. This example is included primarily for verification; the problem is also solved using an optimization approach for comparison. The artery wall is treated as a three-dimensional solid and the continuum inverse element [18, 20] is used. The second example concerns a thin-walled asymmetric aortic aneurysm. Instead of a full 3D analysis, the system is modeled as a shell structure. An inverse shell element developed by the authors [21] is used in the simulation.

2 Open configuration of a cylindrical artery wall

2.1 Inverse solution by finite element method

The finite element formulation of inverse elastostatic problems of a continuum starts from the Eulerian weak form of the static equilibrium problem

$$\int_{\Omega} \sigma_{ij}\eta_{i,j}\mathrm{d}v = \int_{\Omega} \rho b_{\mathrm{i}}\eta_{\mathrm{i}}\mathrm{d}v + \int_{\partial\Omega_t} \bar{t}_{\mathrm{i}}\eta_{\mathrm{i}}\mathrm{d}a, \tag{1}$$

where Ω is the given current configuration, $\boldsymbol{\sigma}$ is the Cauchy stress, $\mathbf{b}$ is the body force, $\bar{\mathbf{t}}$ is the surface traction prescribed on the boundary $\partial\Omega_t$, and $\boldsymbol{\eta}$ is any kinematically admissible variation of the current configuration. The input data for an inverse analysis are the current configuration Ω, the forces $\mathbf{b}$, the boundary traction $\bar{\mathbf{t}}$ and Dirichlet boundary data, if any. The solution for the initial geometry is facilitated via the introduction of the inverse motion $\boldsymbol{\Phi} : \mathbf{X} = \boldsymbol{\Phi}(\mathbf{x})$, which maps a material point at current position $\mathbf{x}$ back to its initial position $\mathbf{X}$. In the formulation proposed by Govindjee and Mihalic [17, 18], the Cauchy stress is parameterized in terms of the inverse deformation gradient $\mathbf{f} := \frac{\partial\boldsymbol{\Phi}}{\partial\mathbf{x}} = \mathbf{F}^{-1}$, where $\mathbf{F}$ is the standard deformation gradient. Upon using the finite element interpolation, the weak form yields a set of nonlinear algebraic equations for the initial nodal positions, which are solved iteratively using a Newton–Raphson procedure. The details of implementation are described in [17, 18, 20].

2.2 Prediction of open configuration

Figure 1 illustrates the BVP considered here. The artery ring is assumed to be in the homeostatic state, the inner and outer radii are $r_{\mathrm{i}} = 2.5421$ mm and $r_{\mathrm{e}} = 2.9138$ mm, respectively, and pressure is assumed to be $p = 100$ mmHg (13.3322 KPa). An imaginary radial cut is applied to the wall

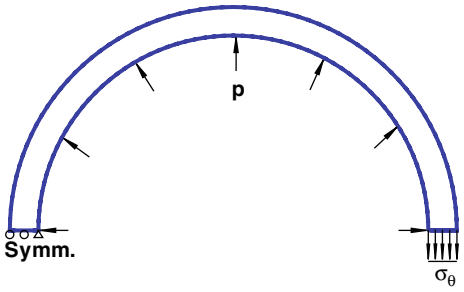

Fig. 1 Schematics of the boundary value problem for determining the opening angle of a cylindrical artery

at the right end, and the ring is sustained in the pre-cut shape by applying on the cut edge a boundary traction that exactly equals the circumferential stress σ_θ in the pre-cut state. The goal of the inverse analysis is to find an open configuration resulted from a simultaneous release of the boundary traction and the internal pressure.

To solve the inverse problem, the stress σ_θ must be determine because it corresponds to the boundary traction in the inverse problem. Following the speculation by Fung and others [11, 12], we assume that σ_θ is uniform across the wall. This assumption enables us to determine σ_θ analytically. Recall that the radial equilibrium equation is governed by

$$\begin{aligned} &\frac{\mathrm{d}\sigma_r}{\mathrm{d}r}+\frac{\sigma_r-\sigma_\theta}{r}=0, \quad r_\mathrm{i}\le r\le r_\mathrm{e},\\ &\sigma_r|_{r=r_\mathrm{i}}=-p, \quad \sigma_r|_{r=r_\mathrm{e}}=0. \end{aligned} \tag{2}$$

When σ_θ is constant, the solution of (2) gives

$$\sigma_\theta=\frac{pr_\mathrm{i}}{r_\mathrm{e}-r_\mathrm{i}}, \quad \sigma_r=\sigma_\theta\left(1-\frac{r_\mathrm{e}}{r}\right). \tag{3}$$

From the given parameters, it is found that $\sigma_\theta = 91.1791$ KPa. A half ring is modeled by 2D solid elements under the plane strain condition. The wall material is assumed to be cylindrical-orthotropic described by a Fung-type energy function [22]

$$W=\frac{c}{2}\mathrm{e}^Q+\frac{\kappa}{2}(J-1)^2, \tag{4}$$

where Q is a quadratic function of the Green–Lagrangian strain $\mathbf{E}=\frac{1}{2}(\mathbf{F}\mathbf{F}^\mathrm{T}-\mathbf{I})$, in components,

$$Q=d_1E_{RR}^2+d_2E_{\Theta\Theta}^2+2d_3E_{RR}E_{\Theta\Theta}+d_4E_{R\Theta}^2. \tag{5}$$

The following material parameters are taken from [2]:

$$\begin{aligned} &c=22.4\,\mathrm{KPa}, \quad d_1=0.0499, \quad d_2=1.0672,\\ &d_3=0.0042, \quad d_4=0.5, \quad \kappa=10,000\,\mathrm{KPa}. \end{aligned}$$

The volumetric term is presented to introduce nearly incompressibility. The material symmetry axes in the deformed state are assumed to align locally with the local cylindrical polar bases ($\mathbf{e}_r$, $\mathbf{e}_\theta$, $\mathbf{e}_z$).

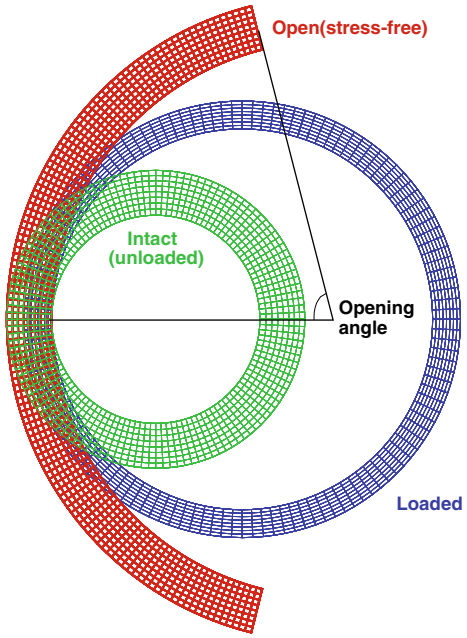

Fig. 2 The origin loaded configuration, the predicted open sector and intact configuration

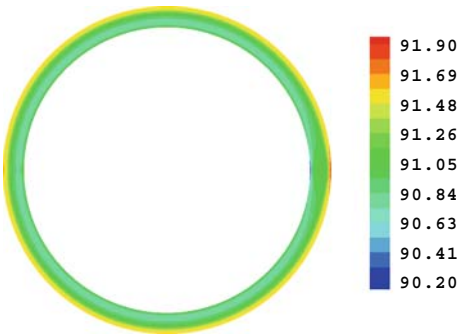

Fig. 3 The circumferential stress σ_θ predicted from the inverse analysis. The values are very close to the assumed uniform value

The inverse analysis predicts an open configuration shown in Fig. 2. Once the open configuration is found, the stress in the homeostatic state can also be computed using the given material model. It should be noted that, the circumferential stress so computed is close to uniform, but not exactly so, as shown in Fig. 3. The inverse motion is not a pure bending, because a pure bending from a perfectly cylindrical sector does not result in a uniform circumferential stress in a Fung material (see Sect. 2.4). Consequently, the open configuration is not perfectly cylindrical, although very close to be so. The inner and outer radii of the cylindrical sector that best fit the open configuration are found to be $R_\mathrm{i} = 3.7115$ mm and $R_\mathrm{e} = 4.3092$ mm, respectively. The best fit opening angle, as defined in Fig. 2, is 75.9°.

2.3 Residual stresses in the intact state

To compute the residual stresses in the unloaded state, a forward finite element analysis is subsequently performed to simulate the closing motion from the open sector. In this analysis, the material symmetry axes are assumed to align locally with the local cylindrical polar basis ($\mathbf{E}_R$, $\mathbf{E}_\Theta$, $\mathbf{E}_Z$) of the best fit sector. The nodes on the open boundary are subject to a displacement control in the vertical direction, and left free in the horizontal direction so that their horizontal positions are determined by equilibrium. The radii of the intact artery are found to be $r_{\mathrm{i}}^0 = 1.3894$ mm and $r_{\mathrm{e}}^0 = 1.9883$ mm. The residual circumferential stresses are plotted in Fig. 4.

2.4 Verification

A simple optimization problem is formulated to estimate the stress-free configuration based on the known homeostatic geometry, the corresponding pressure and the assumption of uniform homeostatic circumferential stress. Consider the forward motion that brings the open sector to the homeostatic configuration, both assumed to be perfectly cylindrical. A material point is denote as (R, Θ, Z) in the stress-free state and (r, θ, z) in the loaded state in cylindrical polar coordinates. The geometry of a stress-free state is completely described by the inner and external radii (R_{i}, R_{e}) and the opening angle Θ_0. Assume that the motion takes the form

$$r = r(R), \quad \theta = \frac{\pi}{\Theta_0}\Theta, \quad z = Z. \tag{6}$$

The principal stretch ratios in the circumferential, longitudinal, and radial directions are, respectively,

$$\lambda_\Theta = \frac{\pi\, r}{\Theta_0 R}, \quad \lambda_Z = 1, \quad \lambda_R = \frac{1}{\lambda_\Theta}, \tag{7}$$

in which the incompressibility condition $\lambda_R\lambda_\Theta\lambda_Z = 1$ is observed. The incompressibility condition alone determines the radial motion to within a constant, giving

$$R = \sqrt{R_{\mathrm{i}}^2 + \frac{\pi}{\Theta_0}(r^2 - r_{\mathrm{i}}^2)}. \tag{8}$$

Equivalently,

$$r = \sqrt{r_{\mathrm{i}}^2 + \frac{\Theta_0}{\pi}(R^2 - R_{\mathrm{i}}^2)}. \tag{9}$$

Considering hyperelastic behavior and incompressibility, the radial and circumferential stresses are given as

$$\sigma_r = \lambda_R^2\frac{\partial W}{\partial E_R} + q, \quad \sigma_\theta = \lambda_\Theta^2\frac{\partial W}{\partial E_\Theta} + q, \tag{10}$$

where $E_I = \frac{1}{2}(\lambda_I^2 - 1)\,(I = R, \Theta, Z)$ are the principal components of Green–Lagrangian strain and q is the unknown hydro-pressure. If σ_θ is uniform, it follows from the equilibrium solution in (3) that

$$\sigma_r - \sigma_\theta = -\frac{p r_{\mathrm{i}} r_{\mathrm{e}}}{r(r_{\mathrm{e}} - r_{\mathrm{i}})}. \tag{11}$$

In light of the constitutive equation in (10), we have

$$\tilde{\Phi} := \lambda_R^2\frac{\partial W}{\partial E_R} - \lambda_\Theta^2\frac{\partial W}{\partial E_\Theta} + \frac{p r_{\mathrm{i}} r_{\mathrm{e}}}{r(r_{\mathrm{e}} - r_{\mathrm{i}})} = 0. \tag{12}$$

Substituting (7) and (8) into this equation, the left side of this equation becomes a function of r that contains two unknown parameters (R_{i}, Θ_0). Since the material constitutive equation involves exponential function, it is

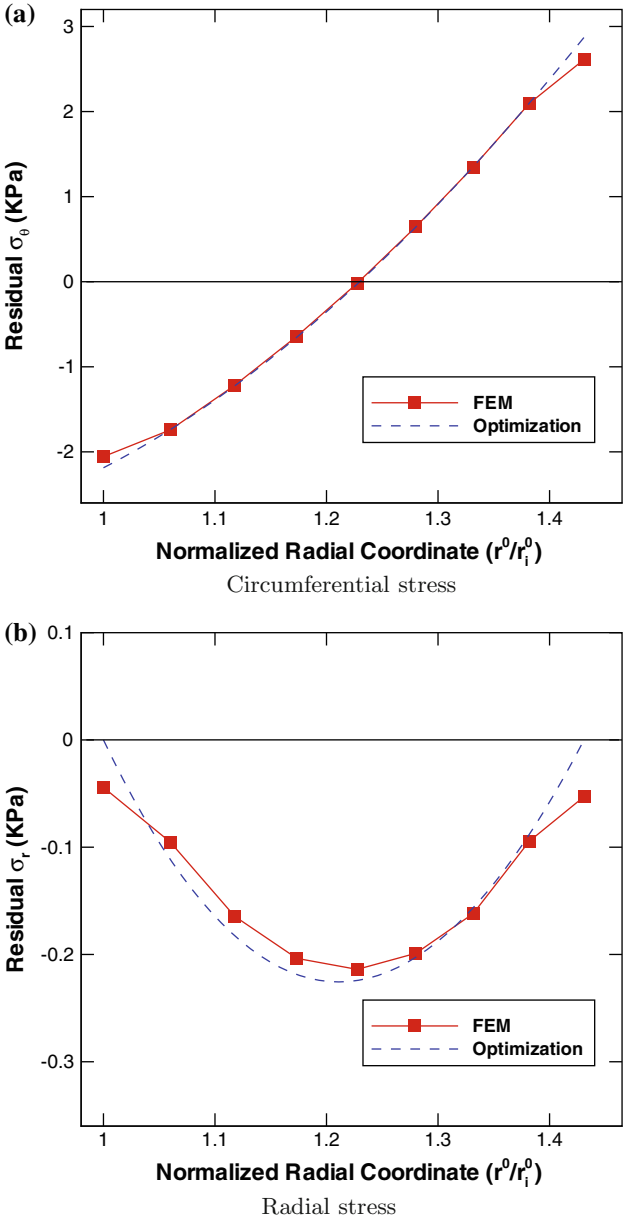

Fig. 4 Comparative radial distribution of the residual stresses in the intact configuration

Table 1 Comparison of the results obtained from finite element inverse method and the optimization method

	R_i (mm)	R_e (mm)	Θ_0(°)	σ_θ (KPa)	r_i^0 (mm)	r_e^0 (mm)
FEM	3.7115	4.3092	75.9000	91.1791 ± 0.8	1.3894	1.9883
Optimization	3.6824	4.2809	76.5892	91.1791 ± 0.4	1.3915	1.9910

R_i, R_e are the inner and external radii and Θ_0 is the opening angle; σ_θ is the circumferential stress in the loaded state; r_i^0 and r_e^0 are the inner and external radii of the intact state

evident that (12) cannot be identically satisfied over the wall thickness regardless of the values of (R_i, Θ_0). An optimization problem is formulated to find the optimal values for R_i and Θ_0. Let the objective function be

$$\hat{\Phi} = \sum_{I=0}^{n} \tilde{\Phi}^2|_{r=(1-\frac{I}{n})r_i+\frac{I}{n}r_e}, \tag{13}$$

where $n + 1$ ($n \geq 1$) is the number of evaluation points along the radial direction; in this example $n = 50$. Solving the problem using *Mathematica* function *NMinimize*, we obtain the best fit opening angle $\Theta_0 = 76.5892$ and inner radius $R_i = 3.6824$. The external radius is computed from (8), giving $R_e = 4.2809$.

A similar procedure is applied to find the residual stresses in the intact state from the predicted open configuration. The goal is to find the radii of the intact artery such that the radial equilibrium equation is satisfied. The equilibrium is governed by (2), but the boundary conditions change to $\sigma_r|_{r=r_i^0} = \sigma_r|_{r=r_e^0} = 0$ due to the absence of internal pressure. Thus the integral of $(2)_1$ gives

$$\sigma_r(r) = \int_{r_i^0}^{r} \frac{\sigma_r - \sigma_\theta}{r} \mathrm{d}r. \tag{14}$$

Consequently

$$\bar{\Phi} := \int_{r_i^0}^{r_e^0} \frac{\sigma_r - \sigma_\theta}{r} \mathrm{d}r = 0. \tag{15}$$

Substituting the constitutive equations in (10), the kinematic relations in (7) and (8), and $r_e^0 = \sqrt{(r_i^0)^2 + \frac{\Theta_0}{\pi}(R_e^2 - R_i^2)}$ into (15) yields an integral function that contains the unknown variable r_i^0. Again, this variable is determined by minimizing the objective function $\check{\Phi} = \bar{\Phi}^2$.

The optimal inner radius of the unloaded configuration is found to be $r_i^0 = 1.3915$ mm. The corresponding external radius is $r_e^0 = 1.9910$ mm. The residual stresses and the hydro-pressure can be found from the three equations in (10) and (14). Table 1 summarizes the results form both the inverse elastostatic method and the optimization method. In overall the results agree well. The comparison of the residual stresses are presented in Fig. 4. It is seen that the circumferential stress distributions are almost identical

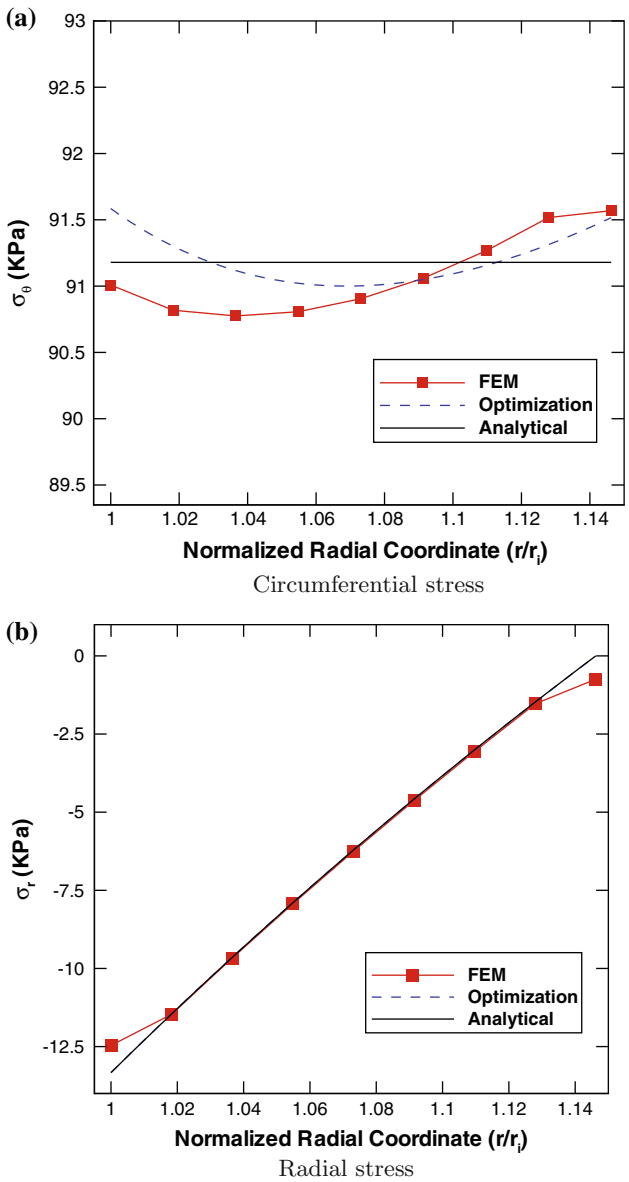

Fig. 5 Comparative radial distributions of the circumferential and radial stresses in the homeostatic state

except at the two ends. The radial stresses also agree well. Figure 5 shows the homeostatic stresses predicted from both approaches. In general, the stresses are in good agreement. The circumferential stresses from both approaches deviate slightly from the assumed uniform

distribution, which is expected because the Fung material cannot produce an exactly uniform circumferential stress in the assumed motion. The optimization method predicts a range of 91–91.5 KPa, while the finite element solution shows a slightly larger variation of 90.75–91.5 KPa.

3 Open configuration of an abdominal aorta aneurysm

To illustrate the application of inverse procedure to thin-walled asymmetric structures, we consider a fusiform abdominal aortic aneurysm (AAA) model shown in Fig. 6. The surface has a mid-section diameter of 6 cm, an axial length of 10.5 cm and is symmetric with respect to the *XZ* plane. The wall thickness is assumed to be the population mean 1.9 mm [23]. The system is modeled as a shell structure. To facilitate the inverse analysis, two basic assumptions are made: (1) the given geometry corresponds to the deformed state under the homeostatic pressure; and (2) in the homeostatic state the wall stress is uniform across the thickness. As is in the continuum case, we also require that the constitutive equation for the material is given. The analysis is conducted using an inverse finite element shell which we describe briefly below.

3.1 Inverse analysis of shell structures

We follow the direct shell theory [24, 25] to describe a thin shell structure. The reference configuration of a shell placed in $\mathbb{R}^3$ is defined as

$$\mathscr{R} := \left\{ \mathbf{X} \in \mathbb{R}^3 | \mathbf{X} = \mathbf{\Phi} + \xi \mathbf{D}, \xi \in \left[-\frac{h}{2}, \frac{h}{2} \right] \right\}, \tag{16}$$

where $\mathbf{\Phi}$ and $\mathbf{D}$ are the position vector of the reference mid-surface and the reference director field, respectively, h is the thickness of the shell. The current, or deformed configuration is specified by

$$\mathscr{C} := \left\{ \mathbf{x} \in \mathbb{R}^3 | \mathbf{x} = \boldsymbol{\varphi} + \xi \mathbf{d}, \xi \in \left[-\frac{h}{2}, \frac{h}{2} \right] \right\}. \tag{17}$$

The local deformation of the shell surface are described by the following measures

$$\begin{aligned} a_{\alpha\beta} &:= \boldsymbol{\varphi}_{,\alpha} \cdot \boldsymbol{\varphi}_{,\beta}, \quad & A_{\alpha\beta} &:= \mathbf{\Phi}_{,\alpha} \cdot \mathbf{\Phi}_{,\beta}, \\ \gamma_\alpha &:= \boldsymbol{\varphi}_{,\alpha} \cdot \mathbf{d}, & \Gamma_\alpha &:= \Phi_{,\alpha} \cdot \mathbf{D}, \\ \kappa_{\alpha\beta} &:= \boldsymbol{\varphi}_{,\alpha} \cdot \mathbf{d}_{,\beta}, & K_{\alpha\beta} &:= \Phi_{,\alpha} \cdot \mathbf{D}_{,\beta}. \end{aligned} \tag{18}$$

where the subscript $(_{,\alpha})$ denotes the derivatives with respect to the surface coordinate $\xi^\alpha (\alpha = 1, 2)$. Here, $a_{\alpha\beta}$ and $A_{\alpha\beta}$ are components of surface metric tensors in $\mathscr{C}$ and $\mathscr{R}$, respectively, γ_α and Γ_α are components of the transverse shear strains in $\mathscr{C}$ and $\mathscr{R}$, and $\kappa_{\alpha\beta}$ and $K_{\alpha\beta}$ are components

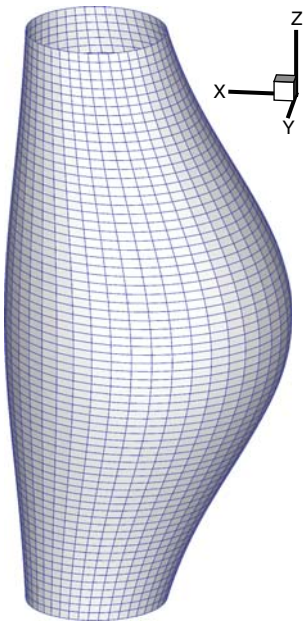

Fig. 6 A fusiform abdominal aorta aneurysm. The mesh is symmetric with respect to the *XZ* plane

of curvature tensors in $\mathscr{C}$ and $\mathscr{R}$. The strain measures can be defined by

$$\begin{aligned} \boldsymbol{\varepsilon} &:= \frac{1}{2}(a_{\alpha\beta} - A_{\alpha\beta})\mathbf{A}^\alpha \otimes \mathbf{A}^\beta, \\ \boldsymbol{\delta} &:= (\gamma_\alpha - \Gamma_\alpha)\mathbf{A}^\alpha, \\ \boldsymbol{\rho} &:= (\kappa_{\alpha\beta} - K_{\alpha\beta})\mathbf{A}^\alpha \otimes \mathbf{A}^\beta, \end{aligned} \tag{19}$$

where $\mathbf{A}_\alpha = \mathbf{\Phi}_{,\alpha}$ are the surface basis vectors in the reference configuration. The basic kinetic variables of the direct shell theory are the effective stress resultant $\tilde{\mathbf{n}} = \tilde{n}^{\alpha\beta}\mathbf{a}_\alpha \otimes \mathbf{a}_\beta$, the effective shear resultant $\tilde{\mathbf{q}} = \tilde{q}^\alpha \mathbf{a}_\alpha$, and the stress couple $\tilde{\mathbf{m}} := \tilde{m}^{\alpha\beta}\mathbf{a}_\alpha \otimes \mathbf{a}_\beta$. Here, $\mathbf{a}_\alpha = \boldsymbol{\varphi}_{,\alpha}$ are the surface basis vectors in the current configuration. The explicit definitions of these resultants are given in [25, 26]. In an elastic shell, the resultants are specified as functions of the deformation measures defined in (18).

Let $\mathbf{\Psi} = (\mathbf{\Phi}, \mathbf{D})$ and $\boldsymbol{\psi} = (\boldsymbol{\varphi}, \mathbf{d})$ denote the reference configuration and the current configuration, respectively, and let $\delta\boldsymbol{\psi}$ denote an admissible variation to the current configuration, the weak form is given as

$$\int_{\mathscr{A}} \left[\frac{1}{2}\tilde{n}^{\alpha\beta}\delta a_{\alpha\beta} + \tilde{m}^{\alpha\beta}\delta\kappa_{\alpha\beta} + \tilde{q}^\alpha \delta\gamma_\alpha \right] \mathrm{d}\mu - G_{\mathrm{ext}}(\delta\boldsymbol{\psi}) = 0, \tag{20}$$

where $G_{\mathrm{ext}}(\delta\boldsymbol{\psi})$ is the virtual work done by external force and moment, and $\mathrm{d}\mu = \sqrt{\det|a_{\alpha\beta}|}\mathrm{d}\xi^1\mathrm{d}\xi^2$. This weak form can facilitate both the forward and the inverse solution. In the forward case, the reference configuration is given while current configuration is sought. The inverse solution pursues exactly the opposite. The weak form is regarded as a

function of the initial configuration. Upon the introduction of the finite element interpolation, the weak form gives rise to a set of nonlinear equations for the referential nodal positions and directors. A brief description of this inverse shell formulation is included in the Appendix. More details can be found in a recent article by the authors [21].

3.2 Homeostatic membrane tension

Similar to the continuum case, we must determine the stress resultant $\tilde{\mathbf{n}}$ along the (hypothetic) cut edge in order to solve the inverse problem. In the context of the shell theory, the assumption of uniform wall stress across thickness implies that the stress couple $\tilde{\mathbf{m}}$ and the effective shear resultant $\tilde{\mathbf{q}}$ vanish. Therefore, at the homeostatic state, the kinetics can be effectively described the membrane theory. It is known that the stress resultant in a pressurized membrane structure is statically determinate. For certain idealized shapes, the resultant can be found analytically [27, 28]. For a general convex membrane structure, the stress resultant can also be determined numerically using the inverse finite element analysis. In the absence of the stress couple and the shear resultant, the weak form in (20) reduces to

$$\int_{\mathscr{A}} \frac{1}{2}\tilde{n}^{\alpha\beta}\delta a_{\alpha\beta}\mathrm{d}\mu - G_{\mathrm{ext}}(\delta\boldsymbol{\psi}) = 0. \tag{21}$$

The finite element procedure for solving the initial geometry from this weak form is a subset of the shell code.

For the AAA problem considered here, the finite element model considers a symmetric half of the AAA. In the membrane analysis, the symmetry boundary condition is applied on the two longitudinal edges. The homeostatic configuration is taken as the input to the inverse membrane analysis. The stress resultant obtained from the membrane solution will be used to provide the traction boundary condition for the shell analysis. Note that in the membrane model the stress couple and the shear resultant are ignored throughout the motion, and therefore, the model is inadequate for determining the open configuration. Indeed, the stress-free configuration resulting from the membrane analysis remains closed.

3.3 Open configuration

The open configuration resulted from a hypothetic cut along the long meridian is predicted. The boundary conditions for the finite element shell model are prescribed as follows: along the short meridian, the symmetry boundary condition is applied. Along the long meridian (where the cut is applied), the stress resultant from the membrane solution is applied while the stress couple is taken to be zero. The model is depicted in Fig. 7. The internal pressure of $p = 100$ mmHg acts on the shell surface.

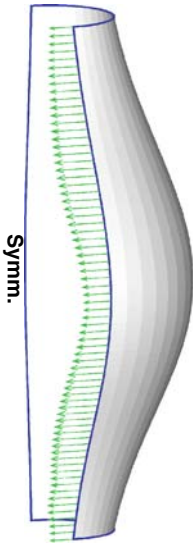

Fig. 7 Schematics of the BVP for the inverse shell analysis. The traction on the open edge is obtained from the membrane analysis The symmetric boundary condition is applied on the other edge

In the simulation, the wall material model is modeled by a two-dimensional Fung energy function

$$\begin{aligned} W &= \frac{c}{2}(\mathrm{e}^{Q} - 1), \\ Q &= d_1E_{11}^2 + d_2E_{22}^2 + 2d_3E_{11}E_{22} + d_4E_{12}^2, \end{aligned} \tag{22}$$

where $E_{\alpha\beta}$ represents the physical components of the Green–Lagrangian strain relative to a local Cartesian basis that aligns with the orthogonal symmetry axes in the reference configuration. By assumption, the base vector $\mathbf{E}_1$ is chosen to coincide with the preferred fiber direction. In a recent review article by Vorp [29] on biomechanics of AAA, the averaged material parameters for AAA are reported based on population-wide biaxial experiment data [30]. Here, we employ a set of modified values using a larger value of c and adding the contribution from the in-plane shear. This particular set of material parameters are

$$\begin{aligned} &c = 1.83, \quad d_1 = 104.9, \quad d_2 = 101.9, \\ &d_3 = 63.2, \quad d_4 = 19.5, \quad f = 28. \end{aligned} \tag{23}$$

The material's preferred direction is assumed to be horizontal and tangent to the surface at every point.

We can introduce a tensor $H^{\alpha\beta\delta\gamma}$ to write the quadratic form Q in the curvilinear system, so that

$$Q = \varepsilon_{\alpha\beta}H^{\alpha\beta\delta\gamma}\varepsilon_{\delta\gamma}. \tag{24}$$

The stress resultant follows the formula $\tilde{n}^{\alpha\beta} = \frac{1}{J}\frac{\partial W}{\partial \varepsilon_{\alpha\beta}}$ where $J = \frac{\sqrt{\det|a_{\alpha\beta}|}}{\sqrt{\det|A_{\alpha\beta}|}}$ is the surface Jacobian, and this gives

$$\tilde{n}^{\alpha\beta} = \frac{c}{J}e^{Q}H^{\alpha\beta\delta\gamma}\varepsilon_{\delta\gamma}. \tag{25}$$

The stress couple and the shear stress are assumed to take the form

$$\tilde{m}^{\alpha\beta} = \frac{ch^2}{6J} f H^{\alpha\beta\delta\gamma}\varepsilon_{\rho\gamma},$$
$$\tilde{q}^{\alpha} = \frac{cd_4}{J} A^{\alpha\beta}\delta_{\beta}. \tag{26}$$

The functional form for the stress couple is motivated by a formula proposed by Schieck et al. [31]. Here, f is a correction factor, which assumes the value of e^{Q} evaluated at a bi-axial strain $E_{11} = E_{22} = 0.1$. The shear resultant function is motived by the corresponding formula for an isotropic material model introduced in [25]. Here, $A^{\alpha\beta}$ are coefficients defined by $A^{\alpha\beta}A_{\beta\gamma} = \delta^{\alpha}{}_{\gamma}$.

Figure 8 presents the predicted open configuration. Since the surface is not axisymmetric, the opening angle varies along the meridian. To evaluate the assumption of uniform stress across the wall thickness, we further computed the stress couple (i.e., moment per unit length) at the homeostatic configuration. The total stress couple,

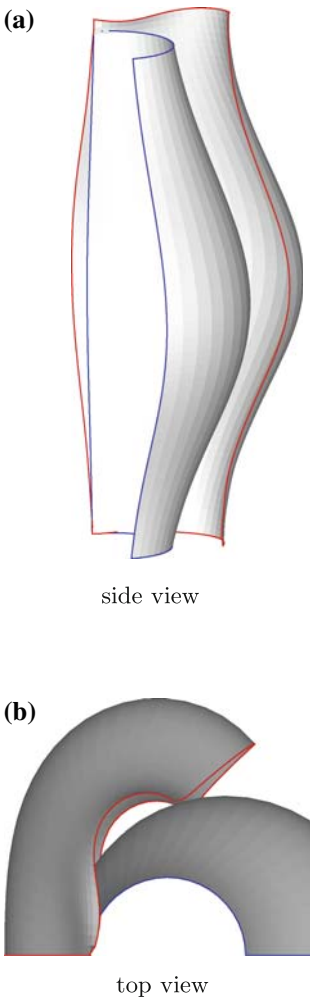

Fig. 8 The predicted open configurations (*red edge*) shown superposed on the homeostatic configuration (*blue edge*)

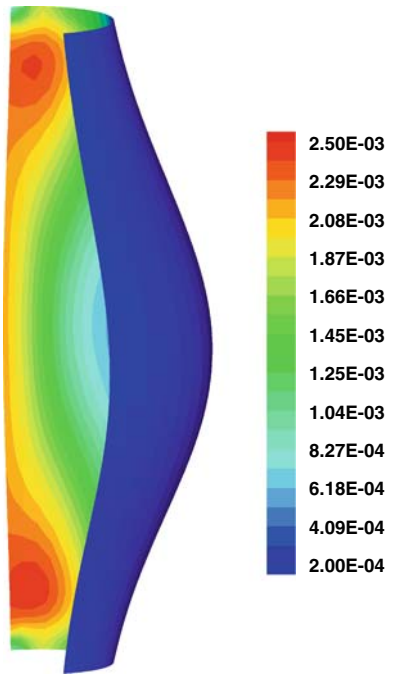

Fig. 9 The total moment $M = \sqrt{M_1^2 + M_2^2}$

defined as $M = \sqrt{M_1^2 + M_2^2}$ where M_1 and M_2 are the principal components, is shown in Fig. 9. It can be seen that the stress couple ranges from 2.0×10^{-4} to 2.5×10^{-3} N. The minimum stress resultant (not shown in plots), denoted by $N_{\min}$, is approximately 0.15 N/mm. Therefore, the stress couple is two to three orders of magnitude smaller than $N_{\min} \times h$. Since a non-zero stress couple indicates stress non-uniformity over the thickness, it is clear that, similar to the continuum case, the inverse shell model does not exactly recover a uniform across-thickness stress. However, the deviation appears to be acceptably small.

4 Concluding remarks

The proposed method hinges on the inverse paradigm of stress analysis. The inverse analysis takes as the input a deformed configuration of an elastic body and the applied load to predict the initial zero-stress configuration of the body. Here, the homeostatic configuration of a tubular vascular organ is taken as the given configuration. In determining the open configuration resulted from a hypothetic cut, it is crucial to obtain the wall stress distribution in the pre-cut state, because it provides the traction boundary condition for the inverse analysis. In this regard, the choice of the homeostatic state as the starting configuration becomes crucially important. We have demonstrated that, under the common assumption

that the homeostatic stress is uniform across the wall thickness, we can determine the wall stress distribution in a cylindrical artery, or the stress resultant in a thin-walled structure. Thus, once the homeostatic geometry and the corresponding pressure are known, an inverse boundary value problem can be formulated. Using this approach, one can predict the open configuration based on information that is readily available from non-invasive measurements.

This method applies to other deformed states as long as the wall stress along the cut boundary can be determined. For example, if the residual stress field in the intact configuration is given a priori by whatever means, the open configuration can be found in the same manner. However, it should be noted that the residual stress in the intact state is typically not known at the onset.

Although the vascular system is considered, the method can be adapted to solve the residual stress problem of other thin-walled organs. Examples of potentially applicable systems include the left ventricle [6, 32, 33], veins [34], intestine, etc. The method is applicable to asymmetric structures, and it is also viable to simulate multiple cuts. Thus, the method has the potential to find a variety of applications.

Acknowledgments We would like to thank Dr. M. L. Raghavan for many helpful discussions. Financial supports from the National Science Foundation Grant CMS 03-48194 and a Research Initiative Grant from the University of Iowa are gratefully acknowledged.

Appendix: Inverse formulation of stress resultant shell

The finite element formulation employs the following interpolations:

$$\begin{aligned} \boldsymbol{\varphi} &= \sum_{I=1}^{\text{nen}} N^I \boldsymbol{\varphi}_I, \quad \mathbf{d} = \sum_{I=1}^{\text{nen}} N^I \mathbf{d}_I, \\ \boldsymbol{\Phi} &= \sum_{I=1}^{\text{nen}} N^I \boldsymbol{\Phi}_I, \quad \mathbf{D} = \sum_{I=1}^{\text{nen}} N^I \mathbf{D}_I, \end{aligned} \tag{27}$$

where I denotes the node number in an element and nen is the total number of nodes per element. It follows that

$$\begin{aligned} \boldsymbol{\varphi}_{,\alpha} &= \sum_{I=1}^{\text{nen}} N^I_{,\alpha} \boldsymbol{\varphi}_I, \quad \mathbf{d}_{,\alpha} = \sum_{I=1}^{\text{nen}} N^I_{,\alpha} \mathbf{d}_I, \\ \boldsymbol{\Phi}_{,\alpha} &= \sum_{I=1}^{\text{nen}} N^I_{,\alpha} \boldsymbol{\Phi}_I, \quad \mathbf{D}_{,\alpha} = \sum_{I=1}^{\text{nen}} N^I_{,\alpha} \mathbf{D}_I. \end{aligned} \tag{28}$$

The deformation measures at Gauss points are computed according to (18). The variations of the Eulerian strain components are

$$\begin{aligned} \delta a_{\alpha\beta} &= \sum_{I=1}^{\text{nen}} \left(N^I_{,\alpha} \delta \boldsymbol{\varphi}_I \cdot \boldsymbol{\varphi}_{,\beta} + N^I_{,\beta} \delta \boldsymbol{\varphi}_I \cdot \boldsymbol{\varphi}_{,\alpha} \right), \\ \delta \kappa_{\alpha\beta} &= \sum_{I=1}^{\text{nen}} \left(N^I_{,\alpha} \delta \boldsymbol{\varphi}_I \cdot \mathbf{d}_{,\beta} + \boldsymbol{\varphi}_{,\alpha} \cdot N^I_{,\beta} \delta \mathbf{d}_I \right), \\ \delta \gamma_\alpha &= \sum_{I=1}^{\text{nen}} \left(N^I_{,\alpha} \delta \boldsymbol{\varphi}_I \cdot \mathbf{d} + \boldsymbol{\varphi}_{,\alpha} \cdot N^I \delta \mathbf{d}_I \right). \end{aligned} \tag{29}$$

The increments of Lagrangian measures under an incremental change of the reference configuration are given as

$$\begin{aligned} \Delta A_{\alpha\beta} &= \sum_{I=1}^{\text{nen}} \left(N^I_{,\alpha} \Delta \boldsymbol{\Phi}_I \cdot \boldsymbol{\Phi}_{,\beta} + N^I_{,\beta} \Delta \boldsymbol{\Phi}_I \cdot \boldsymbol{\Phi}_{,\alpha} \right), \\ \Delta K_{\alpha\beta} &= \sum_{I=1}^{\text{nen}} \left(N^I_{,\alpha} \Delta \boldsymbol{\Phi}_I \cdot \mathbf{D}_{,\beta} + \boldsymbol{\Phi}_{,\alpha} \cdot N^I_{,\beta} \Delta \mathbf{D}_I \right), \\ \Delta \Gamma_\alpha &= \sum_{I=1}^{\text{nen}} \left(N^I_{,\alpha} \Delta \boldsymbol{\Phi}_I \cdot \mathbf{D} + \boldsymbol{\Phi}_{,\alpha} \cdot N^I \Delta \mathbf{D}_I \right). \end{aligned} \tag{30}$$

We employ the geometrically exact algorithm developed by Simo's group for director update. Essentially, one introduces an orthogonal transformation $\boldsymbol{\Lambda}$ such that $\mathbf{D} = \boldsymbol{\Lambda}\mathbf{E}_3$ where $\mathbf{E}_3 = [0,\ 0,\ 1]$. Due to the director inextensibility condition, the increment $\Delta\mathbf{D}$ admits a two-parameter representation given as

$$[\Delta D_1, \Delta D_2, \Delta D_3]^{\mathrm{T}} = \boldsymbol{\Lambda}_{3\times 2} [\Delta T_1, \Delta T_2]^{\mathrm{T}}$$

where $\boldsymbol{\Lambda}_{3\times 2}$ is the matrix obtained by deleting the third column of $\boldsymbol{\Lambda}$. The rotation tensor $\boldsymbol{\Lambda}$ is constructed incrementally during the solution procedure using the geodesic exponential map by Simo and Fox [25] and Simo et al. [26].

We define the "strain-displacement" matrix operators for the reference increment $\Delta\boldsymbol{\Psi}$ as follows:

$$\begin{aligned} \mathbf{B}^{0I}_{\text{m}} &= \begin{bmatrix} \boldsymbol{\Phi}^T_{,1} N^I_{,1} \\ \boldsymbol{\Phi}^T_{,2} N^I_{,2} \\ \boldsymbol{\Phi}^T_{,1} N^I_{,2} + \boldsymbol{\Phi}^T_{,2} N^I_{,1} \end{bmatrix}_{3\times 3} \\ \mathbf{B}^{0I}_{\text{sm}} &= \begin{bmatrix} \mathbf{D}^T N^I_{,1} \\ \mathbf{D}^T N^I_{,2} \end{bmatrix}_{2\times 3}, \quad \mathbf{B}^{0I}_{\text{sb}} = \begin{bmatrix} \boldsymbol{\Phi}^T_{,1} N^I \\ \boldsymbol{\Phi}^T_{,2} N^I \end{bmatrix}_{2\times 3} \boldsymbol{\Lambda}^I_{3\times 2} \\ \mathbf{B}^{0I}_{\text{bm}} &= \begin{bmatrix} \mathbf{D}^T_{,1} N^I_{,1} \\ \mathbf{D}^T_{,2} N^I_{,2} \\ \mathbf{D}^T_{,1} N^I_{,2} + \mathbf{D}^T_{,2} N^I_{,1} \end{bmatrix}_{3\times 3}, \\ \mathbf{B}^{0I}_{\text{bb}} &= \begin{bmatrix} \boldsymbol{\Phi}^T_{,1} N^I_{,1} \\ \boldsymbol{\Phi}^T_{,2} N^I_{,2} \\ \boldsymbol{\Phi}^T_{,1} N^I_{,2} + \boldsymbol{\Phi}^T_{,2} N^I_{,1} \end{bmatrix}_{3\times 3} \boldsymbol{\Lambda}^I_{3\times 2} \end{aligned} \tag{31}$$

where $\boldsymbol{\Lambda}^I$ stands for the rotation tensor at node I. The letters m,s, and b in the subscripts are not free indices but rather

abbreviations for membrane, shear, and bending, respectively. The strain increments in (30) can be written in matrix form as

$$\begin{aligned}
&\left[\frac{1}{2}\Delta A_{11}, \frac{1}{2}\Delta A_{22}, \Delta A_{12}\right]^{\mathrm{T}} = \sum_{I=1}^{\mathrm{nen}} \mathbf{B}_{\mathrm{m}}^{0I}\Delta\boldsymbol{\Phi}^{I},\\
&[\Delta\Gamma_1, \Delta\Gamma_2]^{\mathrm{T}} = \sum_{I=1}^{\mathrm{nen}} \mathbf{B}_{\mathrm{sm}}^{0I}\Delta\boldsymbol{\Phi}_I + \sum_{I=1}^{\mathrm{nen}} \mathbf{B}_{\mathrm{sb}}^{0I}\Delta\mathbf{T}_I,\\
&[\Delta K_{11}, \Delta K_{22}, 2\Delta K_{12}]^{\mathrm{T}} = \sum_{I=1}^{\mathrm{nen}} \mathbf{B}_{\mathrm{bm}}^{0I}\Delta\boldsymbol{\Phi}_I + \sum_{I=1}^{\mathrm{nen}} \mathbf{B}_{\mathrm{bb}}^{0I}\Delta\mathbf{T}_I.
\end{aligned} \tag{32}$$

Similarly, one can also define the matrix operators that relate the variation of ($a_{\alpha\beta}$, γ_α, $\kappa_{\alpha\beta}$) to the configuration variation $\delta\boldsymbol{\psi}$. The operators have the same form as those in (31), but are denoted without the superscript "0", with $(\boldsymbol{\Phi}, \mathbf{D})$ substituted by $(\boldsymbol{\varphi}, \mathbf{d})$, and with $\boldsymbol{\Lambda}$ evaluated at the current director field. Consequently, a form similar to (32) can be established for the variational quantities in (29). Assembling the above matrix operators together, we write

$$\mathbf{B}^{I} = \begin{bmatrix} \mathbf{B}_{\mathrm{m}}^{I} & \mathbf{0}_{3\times 2} \\ \mathbf{B}_{\mathrm{sm}}^{I} & \mathbf{B}_{\mathrm{sb}}^{I} \\ \mathbf{B}_{\mathrm{bm}}^{I} & \mathbf{B}_{\mathrm{bb}}^{I} \end{bmatrix}_{8\times 5}, \quad \mathbf{B}^{0J} = \begin{bmatrix} \mathbf{B}_{\mathrm{m}}^{0J} & \mathbf{0}_{3\times 2} \\ \mathbf{B}_{\mathrm{sm}}^{0J} & \mathbf{B}_{\mathrm{sb}}^{0J} \\ \mathbf{B}_{\mathrm{bm}}^{0J} & \mathbf{B}_{\mathrm{bb}}^{0J} \end{bmatrix}_{8\times 5}. \tag{33}$$

Introducing the element stress resultant vector

$$\mathbf{R} = \left[\tilde{n}^{11}, \tilde{n}^{22}, \tilde{n}^{12}, \tilde{q}^{1}, \tilde{q}^{2}, \tilde{m}^{11}, \tilde{m}^{22}, \tilde{m}^{12}\right]^{T}, \tag{34}$$

The weak form can be written as

$$G(\boldsymbol{\psi}, \boldsymbol{\Psi}; \delta\boldsymbol{\psi}) = [\delta\boldsymbol{\varphi}^{T}, \delta\mathbf{T}^{T}] \int_{\mathscr{A}} \mathbf{B}^{T}\mathbf{R}\mathrm{d}\mu - G_{\mathrm{ext}}(\delta\boldsymbol{\psi}) = 0, \tag{35}$$

where $\mathbf{B} = [\mathbf{B}^1, \mathbf{B}^2, ..., \mathbf{B}^{\mathrm{nen}}]_{8\times(5\times\mathrm{nen})}$ is the assembled element strain-displacement matrix and $[\delta\boldsymbol{\varphi}^T, \delta\mathbf{T}^T] = [\delta\boldsymbol{\varphi}_1^T, \delta\mathbf{T}_1^T, \delta\boldsymbol{\varphi}_2^T, \delta\mathbf{T}_2^T, \ldots, \delta\boldsymbol{\varphi}_{\mathrm{nen}}^T, \delta\mathbf{T}_{\mathrm{nen}}^T]_{1\times(5\times\mathrm{nen})}$. This vectorized weak form is exactly the same as the one used by Simo and Fox [25] for forward analysis, except now the deformed configuration is given. The finite element equation can be written as

$$\int_{\mathscr{A}} \mathbf{B}^{T}\mathbf{R}\mathrm{d}\mu - \mathbf{F}^{\mathrm{ext}} = \mathbf{0}. \tag{36}$$

In the inverse analysis the finite element equation is solved to determined the referential nodal positions $\boldsymbol{\Phi}_I$ and the referential director $\mathbf{D}_I$. A Newton–Raphson procedure is employed, in which the equation (36) is linearized with respect to $\boldsymbol{\Phi}_I$ and $\mathbf{D}_I$. In an elastic shell, the resultants $(\tilde{n}^{\alpha\beta}, \tilde{q}^{\alpha}, \tilde{m}^{\alpha\beta})$ are specified as functions of the deformation measures introduced in (18). We introduces the material tensor $\mathbb{C}$ such that

$$\Delta\mathbf{R} = \mathbb{C}\Delta\mathbf{e}, \tag{37}$$

where

$$\Delta\mathbf{e} = \left[\frac{1}{2}\Delta A_{11}, \frac{1}{2}\Delta A_{11}, \Delta A_{12}, \Delta\Gamma_1, \Delta\Gamma_2, \Delta K_{11}, \Delta K_{22}, 2\Delta K_{12}\right]^{T}. \tag{38}$$

The linearization of the finite element equation yields the element stiffness matrix

$$K_{IJ} = \int_{\mathscr{A}} (\mathbf{B}^{I})^{T}\mathbb{C}\mathbf{B}^{0J}\mathrm{d}\mu. \tag{39}$$

References

1. Chuong CJ, Fung YC (1986) Residual stress in arteries. In: Schmid-Schonbein GW, Woo SLY, Zweifach BW (eds) Frontiers in biomechanics. Springer, New York, pp 117–129
2. Chuong CJ, Fung YC (1986) On residual-stresses in arteries. J Biomech Eng Trans ASME 108:189–192
3. Vaishnav RN, Vossoughi J (1983) Estimation of residual strains in aortic segments. In: Hall CW (ed) Biomedical engineering II. Recent developments. Pergamon Press, New York, pp 330–333
4. Vaishnav RN, Vossoughi J (1987) Residual stress and strain in aortic segments. J Biomech 20:235–237
5. Fung YC (1987) Residual-stresses in heart and blood-vessels—evidences and significance. Fed Proc 46:498–498
6. Omens JH, Fung YC (1990) Residual strain in rat left ventricle. Circ Res 66:37–45
7. Fung YC (1991) What are the residual-stresses doing in our blood-vessels. Ann Biomed Eng 19:237–249
8. Vossoughi J, Hedjazi Z, Borris FS II (1993) Intimal residual stress and strain in large arteries. In: Langrana NA, Friedman MH, Grood ES (eds) Proceedings of summer bioengineering conference. ASME, New York, pp 434–437
9. Greenwald SE, Moore JE, Rachev A, Kane TPC, Meister JJ (1997) Experimental investigation of the distribution of residual strains in the artery wall. J Biomech Eng Trans ASME 119:438–444
10. Gregersen H (2000) Residual strain in the gastrointestinal tract: a new concept. Neurogastroenterol Motil 12:411–414
11. Fung YC (1985) What principle governs the stress distribution in living organs. In: Fung YC, Fukada E, Wang JJ (eds) Biomechanics in China, Japan and U.S.A. Science Press, Beijing, pp 1–13
12. Rachev A, Greenwald SE (2003) Residual strains in conduit arteries. J Biomech 36:661–670
13. Van Dyke TJ, Hoger A (2002) A new method for predicting the opening angle for soft tissues. ASME J Biomech Eng 124:347–354
14. Taber LA, Eggers DW (1996) Theoretical study of stress-modulated growth in the aorta. J Theor Biol 180:343–357
15. Stalhand J, Klarbring A, Karlsson M (2004) Towards in vivo aorta material identification and stress estimation. Biomech Model Mechanobiol 2:169–186
16. Olsson T, Stalhand J, Klarbring A (2006) Modeling initial strain distribution in soft tissues with application to arteries. Biomech Model Mechanobiol 5:27–38
17. Govindjee S, Mihalic PA (1996) Computational methods for inverse finite elastostatics. Comput Methods Appl Mech Eng 136:47–57
18. Govindjee S, Mihalic PA (1998) Computational methods for inverse deformations in quasi-incompressible finite elasticity. Int J Numer Methods Eng 43:821–838

19. Lu J, Zhou X, Raghavan ML (2007) Inverse elastostatic stress analysis in pre-deformed biological structures: demonstration using abdominal aortic aneurysm. J Biomech 40:693–696
20. Lu J, Zhou X, Raghavan ML (2007) Computational method of inverse elastostatics for anisotropic hyperelastic solids. Int J Numer Methods Eng 69:1239–1261
21. Zhou X, Lu J (2008) Inverse formulation for geometrically exact stress resultant shells. Int J Numer Methods Eng 74:1278–1302
22. Fung YC (1993) Biomechanics: mechanical properties of living tissues, 2nd edn. Springer, Berlin
23. Raghavan ML, Vorp DA (2000) Toward a biomechanical tool to evaluate rupture potential of abdominal aortic aneurysm: identification of a finite strain constitutive model and evaluation of its applicability. J Biomech 33:475–482
24. Naghdi PM (1972) The theory of plates and shells. In: Truesdell C (ed) Handbuch der Physik, vol VIa/2. Springer, Berlin, pp 425–640
25. Simo JC, Fox DD (1989) On a stress resultant geometrically exact shell model. Part I. Formulation and optimal parametrization. Comput Methods Appl Mech Eng 72(3):267–304
26. Simo JC, Fox DD, Rifai MS (1990) On a stress resultant geometrically exact shell model. Part III: Computational aspects of the nonlinear-theory. Comput Methods Appl Mech Eng 79:21–70
27. Elger DF, Blackketter DM, Budwig RS, Johansen KH (1996) The influence of shape on the stresses in model abdominal aortic aneurysms. J Biomech Eng Trans ASME 118:326–332
28. Humphrey JD (2002) Cardiovascular solid mechanics. Springer, New York
29. Vorp DA (2007) Biomechanics of abdominal aortic aneurysm. J Biomech 40:1887–1902
30. Vande Geest JP, Sacks MS, Vorp DA (2006) The effects of aneurysm on the biaxial mechanical behavior of human abdominal aorta. J Biomech 39:1324–1334
31. Schieck B, Pietraszkiewicz W, Stumpf H (1992) Theory and numerical analysis of shells undergoing large elastic strains. Int J Solids Struct 29:689–709
32. Omens JH, Vaplon SM, Fazeli B, McCulloch AD (1998) Left ventricular geometric remodeling and residual stress in the rat heart. J Biomech Eng Trans ASME 120:715–719
33. Omens JH, McCulloch AD, Criscione JC (2003) Complex distributions of residual stress and strain in the mouse left ventricle: experimental and theoretical models. Biomech Model Mechanobiol 1:267–277
34. Xie JP, Liu SQ, Yang RF, Fung YC (1991) The zero-stress state of rat veins and vena cava. J Biomech Eng Trans ASME 113:36–41